

Yields and elliptic flow of $d(\bar{d})$ and ${}^3\text{He}(\overline{{}^3\text{He}})$ in Au+Au collisions at $\sqrt{s_{NN}} = 200$ GeV

B. I. Abelev^h, M. M. Aggarwal^{ad}, Z. Ahammed^{au},
 A. V. Alakhverdyants^k, B. D. Anderson^r, D. Arkhipkin^ℓ,
 G. S. Averichev^k, J. Balewski^v, O. Barannikova^h,
 L. S. Barnby^b, J. Baudot^p, S. Baumgart^{ba}, D. R. Beavis^c,
 R. Bellwied^{ay}, F. Benedosso^{aa}, M. J. Betancourt^v,
 R. R. Betts^h, A. Bhasin^q, A. K. Bhati^{ad}, H. Bichsel^{aw},
 J. Bielcik^j, J. Bielcikova^j, B. Biritz^f, L. C. Bland^c, I. Bnzarov^k,
 M. Bombara^b, B. E. Bonner^{aj}, J. Bouchet^r, E. Braidot^{aa},
 A. V. Brandin^y, E. Bruna^{ba}, S. Buehlmann^{ac}, T. P. Burton^b,
 M. Bystersky^j, X. Z. Cai^{an}, H. Caines^{ba}, M. Calderon^e,
 O. Catu^{ba}, D. Cebra^e, R. Cendejas^f, M. C. Cervantes^{ap},
 Z. Chajecki^{ab}, P. Chaloupka^j, S. Chattopadhyay^{au},
 H. F. Chen^{al}, J. H. Chen^r, J. Y. Chen^{az}, J. Cheng^{ar},
 M. Cherneyⁱ, A. Chikanian^{ba}, K. E. Choi^{ah}, W. Christie^c,
 R. F. Clarke^{ap}, M. J. M. Coddington^{ap}, R. Corliss^v,
 T. M. Cormier^{ay}, M. R. Cosentino^{ak}, J. G. Cramer^{aw},
 H. J. Crawford^d, D. Das^e, S. Dash^m, M. Daugherty^{aq},
 L. C. De Silva^{ay}, T. G. Dedovich^k, M. DePhillips^c,
 A. A. Derevschikov^{af}, R. Derradi de Souza^g, L. Didenko^c,
 P. Djawotho^{ap}, S. M. Dogra^q, X. Dong^u, J. L. Drachenberg^{ap},
 J. E. Draper^e, J. C. Dunlop^c, M. R. Dutta Mazumdar^{au},
 L. G. Efimov^k, E. Elhalhuli^b, M. Elnimr^{ay}, V. Emelianov^y,
 J. Engelage^d, G. Eppley^{aj}, B. Erasmus^{ao}, M. Estienne^{ao},
 L. Eun^{ae}, P. Fachini^c, R. Fatemi^s, J. Fedorisin^k, A. Feng^{az},
 P. Filip^ℓ, E. Finch^{ba}, V. Fine^c, Y. Fisyak^c, C. A. Gagliardi^{ap},
 L. Gaillard^b, D. R. Gangadharan^f, M. S. Ganti^{au},
 E. J. Garcia-Solis^h, A. Geromitsos^{ao}, F. Geurts^{aj},
 V. Ghazikhanian^f, P. Ghosh^{au}, Y. N. Gorbunovⁱ, A. Gordon^c,
 O. Grebenyuk^u, D. Grosnick^{at}, B. Grube^{ah}, S. M. Guertin^f,
 K. S. F. F. Guimaraes^{ak}, A. Gupta^q, N. Gupta^q, W. Guryn^c,

B. Haag^e, T. J. Hallman^c, A. Hamed^{ap}, J. W. Harris^{ba},
 W. He^o, M. Heinz^{ba}, S. Heppelmann^{ae}, B. Hippolyte^p,
 A. Hirsch^{ag}, E. Hjort^u, A. M. Hoffman^v, G. W. Hoffmann^{aq},
 D. J. Hofman^h, R. S. Hollis^h, H. Z. Huang^f, T. J. Humanic^{ab},
 L. Huo^{ap}, G. Igo^f, A. Iordanova^h, P. Jacobs^u, J. W. W. Jacobs,
 P. Jakl^j, C. Jena^m, F. Jin^{an}, C. L. Jones^v, P. G. Jones^b,
 J. Joseph^r, E. G. Judd^d, S. Kabana^{ao}, K. Kajimoto^{aq},
 K. Kang^{ar}, J. Kapitan^j, K. Kauder^h, D. Keane^r,
 A. Kechechyan^k, D. Kettler^{aw}, V. Yu. Khodyrev^{af},
 D. P. Kikola^u, J. Kiryluk^u, A. Kisiel^{ab}, S. R. Klein^u,
 A. G. Knospe^{ba}, A. Kocoloski^v, D. D. Koetke^{at}, J. Konzer^{ag},
 M. Kopytine^r, I. Koralt^{ac}, W. Korsch^s, L. Kotchenda^y,
 V. Kouchpil^j, P. Kravtsov^y, V. I. Kravtsov^{af}, K. Krueger^a,
 M. Krus^j, C. Kuhn^p, L. Kumar^{ad}, P. Kurnadi^f,
 M. A. C. Lamont^c, J. M. Landgraf^c, S. LaPointe^{ay}, J. Lauret^c,
 A. Lebedev^c, R. Lednicky^l, C-H. Lee^{ah}, J. H. Lee^c,
 W. Leight^v, M. J. LeVine^c, C. Li^{al}, N. Li^{az}, Y. Li^{ar}, G. Lin^{ba},
 S. J. Lindenbaum^z, M. A. Lisa^{ab}, F. Liu^{az}, H. Liu^e, J. Liu^{aj},
 L. Liu^{az}, T. Ljubicic^c, W. J. Llope^{aj}, R. S. Longacre^c,
 W. A. Love^c, Y. Lu^{al}, T. Ludlam^c, G. L. Ma^{an}, Y. G. Ma^{an},
 D. P. Mahapatra^m, R. Majka^{ba}, O. I. Mall^e, L. K. Mangotra^q,
 R. Manweiler^{at}, S. Margetis^r, C. Markert^{aq}, H. Masui^u,
 H. S. Matis^u, Yu. A. Matulenko^{af}, D. McDonald^{aj},
 T. S. McShaneⁱ, A. Meschanin^{af}, R. Milner^v, N. G. Minaev^{af},
 S. Mioduszewski^{ap}, A. Mischke^{aa}, B. Mohanty^{au},
 D. A. Morozov^{af}, M. G. Munhoz^{ak}, B. K. Nandiⁿ,
 C. Natrass^{ba}, T. K. Nayak^{au}, J. M. Nelson^b,
 P. K. Netrakanti^{ag}, M. J. Ng^d, L. V. Nogach^{af},
 S. B. Nurushev^{af}, G. Odyniec^u, A. Ogawa^c, H. Okada^c,
 V. Okorokov^y, D. Olson^u, M. Pachr^j, B. S. Page^o, S. K. Pal^{au},
 Y. Pandit^r, Y. Panebratsev^k, T. Pawlak^{av}, T. Peitzmann^{aa},
 V. Perevoztchikov^c, C. Perkins^d, W. Peryt^{av}, S. C. Phatak^m,
 P. Pile^c, M. Planinic^{bb}, M. A. Ploskon^u, J. Pluta^{av},
 D. Plyku^{ac}, N. Poljak^{bb}, A. M. Poskanzer^u,
 B. V. K. S. Potukuchi^q, D. Prindle^{aw}, C. Pruneau^{ay},

N. K. Pruthi^{ad}, P. R. Pujahariⁿ, J. Putschke^{ba}, R. Raniwala^{ai},
 S. Raniwala^{ai}, R. L. Ray^{aq}, R. Redwine^v, R. Reed^e,
 A. Ridiger^y, H. G. Ritter^u, J. B. Roberts^{aj},
 O. V. Rogachevskiy^k, J. L. Romero^e, A. Rose^u, C. Roy^{ao},
 L. Ruan^c, M. J. Russcher^{aa}, R. Sahoo^{ao}, S. Sakai^f,
 I. Sakrejda^u, T. Sakuma^v, S. Salur^u, J. Sandweiss^{ba},
 M. Sarsour^{ap}, J. Schambach^{aq}, R. P. Scharenberg^{ag},
 N. Schmitz^w, J. Segerⁱ, I. Selyuzhenkov^o, P. Seyboth^w,
 A. Shabetai^p, E. Shahaliev^k, M. Shao^{al}, M. Sharma^{ay},
 S. S. Shi^{az}, X-H. Shi^{an}, E. P. Sichtermann^u, F. Simon^w,
 R. N. Singaraju^{au}, M. J. Skoby^{ag}, N. Smirnov^{ba}, P. Sorensen^c,
 J. Sowinski^o, H. M. Spinka^a, B. Srivastava^{ag},
 T. D. S. Stanislaus^{at}, D. Staszak^f, M. Strikhanov^y,
 B. Stringfellow^{ag}, A. A. P. Suaide^{ak}, M. C. Suarez^h,
 N. L. Subba^r, M. Sumbera^j, X. M. Sun^u, Y. Sun^{al}, Z. Sun^t,
 B. Surov^v, T. J. M. Symons^u, A. Szanto de Toledo^{ak},
 J. Takahashi^g, A. H. Tang^c, Z. Tang^{al}, T. Tarini^{ay},
 T. Tarnowsky^x, D. Thein^{aq}, J. H. Thomas^u, J. Tian^{an},
 A. R. Timmins^{ay}, S. Timoshenko^y, D. Tlusty^j, M. Tokarev^k,
 T. A. Trainor^{aw}, V. N. Tram^u, A. L. Trattner^d,
 S. Trentalange^f, R. E. Tribble^{ap}, O. D. Tsai^f, J. Ulery^{ag},
 T. Ullrich^c, D. G. Underwood^a, G. Van Buren^c,
 M. van Leeuwen^{aa}, G. van Nieuwenhuizen^v,
 J. A. Vanfossen, Jr.^r, R. Varma^o, G. M. S. Vasconcelos^g,
 A. N. Vasiliev^{af}, F. Videbaek^c, S. E. Vigdor^o, Y. P. Viyogi^m,
 S. Vokal^k, S. A. Voloshin^{ay}, M. Wada^{aq}, M. Walker^v,
 F. Wang^{ag}, G. Wang^f, H. Wang^x, J. S. Wang^t, Q. Wang^{ag},
 X. Wang^{ar}, X. L. Wang^{al}, Y. Wang^{ar}, G. Webb^s,
 J. C. Webb^{at}, G. D. Westfall^x, C. Whitten Jr.^f, H. Wieman^u,
 S. W. Wissink^o, R. Witt^{as}, Y. Wu^{az}, W. Xie^{ag}, N. Xu^u,
 Q. H. Xu^{am}, Y. Xu^{al}, Z. Xu^c, Y. Yang^t, P. Yepes^{aj}, K. Yip^c,
 I-K. Yoo^{ah}, Q. Yue^{ar}, M. Zawisza^{av}, H. Zbroszczyk^{av},
 W. Zhan^t, S. Zhang^{an}, W. M. Zhang^r, X. P. Zhang^u,
 Y. Zhang^u, Z. P. Zhang^{al}, Y. Zhao^{al}, C. Zhong^{an}, J. Zhou^{aj},
 X. Zhu^{ar}, R. Zoulkarneev^l, Y. Zoulkarneeva^l and J. X. Zuo^{an}

(STAR Collaboration)

- ^aArgonne National Laboratory, Argonne, Illinois 60439, USA
^bUniversity of Birmingham, Birmingham, United Kingdom
^cBrookhaven National Laboratory, Upton, New York 11973, USA
^dUniversity of California, Berkeley, California 94720, USA
^eUniversity of California, Davis, California 95616, USA
^fUniversity of California, Los Angeles, California 90095, USA
^gUniversidade Estadual de Campinas, Sao Paulo, Brazil
^hUniversity of Illinois at Chicago, Chicago, Illinois 60607, USA
ⁱCreighton University, Omaha, Nebraska 68178, USA
^jNuclear Physics Institute AS CR, 250 68 Řež/Prague, Czech Republic
^kLaboratory for High Energy (JINR), Dubna, Russia
^lParticle Physics Laboratory (JINR), Dubna, Russia
^mInstitute of Physics, Bhubaneswar 751005, India
ⁿIndian Institute of Technology, Mumbai, India
^oIndiana University, Bloomington, Indiana 47408, USA
^pInstitut de Recherches Subatomiques, Strasbourg, France
^qUniversity of Jammu, Jammu 180001, India
^rKent State University, Kent, Ohio 44242, USA
^sUniversity of Kentucky, Lexington, Kentucky, 40506-0055, USA
^tInstitute of Modern Physics, Lanzhou, China
^uLawrence Berkeley National Laboratory, Berkeley, California 94720, USA
^vMassachusetts Institute of Technology, Cambridge, MA 02139-4307, USA
^wMax-Planck-Institut für Physik, Munich, Germany
^xMichigan State University, East Lansing, Michigan 48824, USA
^yMoscow Engineering Physics Institute, Moscow Russia
^zCity College of New York, New York City, New York 10031, USA
^{aa}NIKHEF and Utrecht University, Amsterdam, The Netherlands
^{ab}Ohio State University, Columbus, Ohio 43210, USA
^{ac}Old Dominion University, Norfolk, VA, 23529, USA
^{ad}Panjab University, Chandigarh 160014, India
^{ae}Pennsylvania State University, University Park, Pennsylvania 16802, USA
^{af}Institute of High Energy Physics, Protvino, Russia
^{ag}Purdue University, West Lafayette, Indiana 47907, USA
^{ah}Pusan National University, Pusan, Republic of Korea
^{ai}University of Rajasthan, Jaipur 302004, India

- ^{aj}*Rice University, Houston, Texas 77251, USA*
- ^{ak}*Universidade de Sao Paulo, Sao Paulo, Brazil*
- ^{al}*University of Science & Technology of China, Hefei 230026, China*
- ^{am}*Shandong University, Jinan, Shandong 250100, China*
- ^{an}*Shanghai Institute of Applied Physics, Shanghai 201800, China*
- ^{ao}*SUBATECH, Nantes, France*
- ^{ap}*Texas A&M University, College Station, Texas 77843, USA*
- ^{aq}*University of Texas, Austin, Texas 78712, USA*
- ^{ar}*Tsinghua University, Beijing 100084, China*
- ^{as}*United States Naval Academy, Annapolis, MD 21402, USA*
- ^{at}*Valparaiso University, Valparaiso, Indiana 46383, USA*
- ^{au}*Variable Energy Cyclotron Centre, Kolkata 700064, India*
- ^{av}*Warsaw University of Technology, Warsaw, Poland*
- ^{aw}*University of Washington, Seattle, Washington 98195, USA*
- ^{ay}*Wayne State University, Detroit, Michigan 48201, USA*
- ^{az}*Institute of Particle Physics, CCNU (HZNU), Wuhan 430079, China*
- ^{ba}*Yale University, New Haven, Connecticut 06520, USA*
- ^{bb}*University of Zagreb, Zagreb, HR-10002, Croatia*

Abstract

We present the p_T spectra, elliptic flow (v_2) and coalescence parameters B_2 for d , \bar{d} ($1 < p_T < 4$ GeV/c) and B_3 for ${}^3\text{He}$, $\overline{{}^3\text{He}}$ ($2 < p_T < 6$ GeV/c) produced at mid-rapidity in Au+Au collisions at $\sqrt{s_{NN}} = 200$ GeV. The results are measured in the STAR experiment at RHIC. The spectra of the light nuclei show softer p_T distributions than calculations from a blast-wave model in which the parameters were fixed from pion, kaon and proton $v_2(p_T)$ and p_T distributions. The coalescence volume is found to track with pion HBT results for different collision geometries. The v_2 measurement for $d(\bar{d})$ as a function of transverse momentum p_T is found to follow an approximate atomic mass number (A) scaling while that of ${}^3\text{He}(\overline{{}^3\text{He}})$ deviates slightly from the scaling. A negative v_2 has been observed for \bar{d} at low p_T , consistent with large radial flow in Au+Au collisions.

Key words:

1 Introduction

In relativistic heavy ion collisions, light nuclei and anti-nuclei are formed through coalescence of produced nucleons and anti-nucleons or participant nucleons [1,2,3]. Since the binding energy is small, this formation process can only happen at a late stage of the evolution of the system when interactions between nucleons and other particles are weak. This process is called final-state coalescence [1,4]. The coalescence probability is related to the local nucleon density. Therefore, the production of light nuclei provides a tool to measure collective motion and freeze-out properties, such as particle density [5] and correlation volume.

Invariant yields for the production of nuclei can be related [1] to the primordial yields of nucleons by Equation 1.

$$E_A \frac{d^3 N_A}{d^3 p_A} = B_A (E_p \frac{d^3 N_p}{d^3 p_p})^Z (E_n \frac{d^3 N_n}{d^3 p_n})^{A-Z} \approx B_A (E_p \frac{d^3 N_p}{d^3 p_p})^A \quad (1)$$

where N_A , N_p , and N_n denote the yields of the particular nucleus, and of its constituent protons and neutrons, respectively. B_A is the coalescence parameter. $E \frac{d^3 N}{d^3 p}$ is the invariant yield of nucleons or nuclei; A and Z are the atomic mass number and atomic number, respectively; p_A , p_p and p_n are the momenta of the nuclei, protons and neutrons, respectively, where $p_A = A \cdot p_p$ is assumed. The coalescence parameter, B_A , is related to the freeze-out correlation volume [1]: $B_A \propto V_f^{1-A}$. For an expanding fireball, the effective homogeneous coalescence volume decreases with transverse mass and temperature (M_t/T) as detailed in Ref. [2].

On the other hand, a blast-wave model is often used to describe the spectra of identified particles produced in relativistic heavy ion collisions [6,7]. In this model, the particle spectra are determined by global parameters (temperature, flow profile) and particle mass. Up to now, hydrodynamic model simulations or blast-wave fits to the data only included elementary particles without any composite elements, such as nuclei [6]. Experimental measurements can be used to provide insights into whether the homogeneous volume (as in a coalescence picture) or mass (as in a blast-wave model) has a bigger influence on the yields of nuclei in heavy ion collisions.

In the case of deuteron production at low p_T , $B_2 \propto 1/V_f$. The ratio of deuteron yield over proton yield at the same p_T/A (denoted as d/p , and \bar{d}/\bar{p} for anti-deuteron), is proportional to the baryon density [5,8]. This is analogous to the deuteron to hydrogen ratio (D/H) measurements of Big-Bang nucleosynthesis (BBN), which is a very sensitive probe of baryon abundance in the early universe [9,10]. Although both processes are sensitive to the baryon density, the

processes themselves are very different. In coalescence, a proton and a neutron form a deuteron due to the overlap of the quantum wave function in a dilute QCD medium, while in BBN the deuteron production is through $p(n,\gamma)D$ photo-production. Nevertheless, it is interesting to investigate whether the coalescence at much higher temperature and density, which existed also at the pre-BBN stage of the early universe, produces a dramatically different deuteron abundance when compared to the photo-production of deuterium in the standard BBN model.

Coalescence has been generalized as a mechanism for partons to form hadrons at an early stage of heavy ion collisions [11,12]. It is experimentally difficult to study how local correlations and energy/entropy play a role in coalescence at the partonic level since the constituents are not directly observable. By studying the spectra and elliptic flow of nuclei and comparing to those of their constituents (nucleons), we have a better handle on how coalescence happens. It has been found that elliptic flow (v_2) of hadrons is very sensitive to their underlying partonic degrees of freedom [13,11]. An analog in nucleus production is to test if nucleus elliptic flow scales with the atomic mass number (A). Deviations may point to a non-uniform nucleon distribution with respect to the collision geometry or large nuclear density fluctuations. This will provide valuable data for studying the freeze-out dynamics and coalescence mechanism in general.

Previously, measurements of nucleus production at RHIC suffered from low statistics. The first observation of anti-helium [14] at RHIC and measurements of coalescence properties [15] with (anti-)deuterons at RHIC have been previously published. More recently, increasing RHIC luminosity and detector upgrades allow more precise measurements of yield and elliptic flow of nuclei. In this paper, we present spectra and v_2 of the deuteron, 3He , and their anti-particles (\bar{d} and ${}^3\bar{He}$). We compare volumes extracted from nucleus production and from pion HBT. First measurements of 3He v_2 and high statistics \bar{d} v_2 at low p_T will be presented and their implications will be discussed.

2 Experiment and analysis

The data presented here are obtained from the Time Projection Chamber (TPC) [16] and the Time-Of-Flight (TOF) detectors [17] in the STAR experiment at RHIC in the year 2004. The TOF detector system was a prototype module covering $\pi/30$ rad in azimuth and $-1.0 < \eta < 0$ in pseudorapidity. These analyses used a data sample of 25 million central triggered events (0-12% centrality) and 24 million minimum-bias triggered events (0-80% centrality) and TOF information is available for 16 million central and 15 million minimum-bias events. The selection of centrality is based on the Glauber

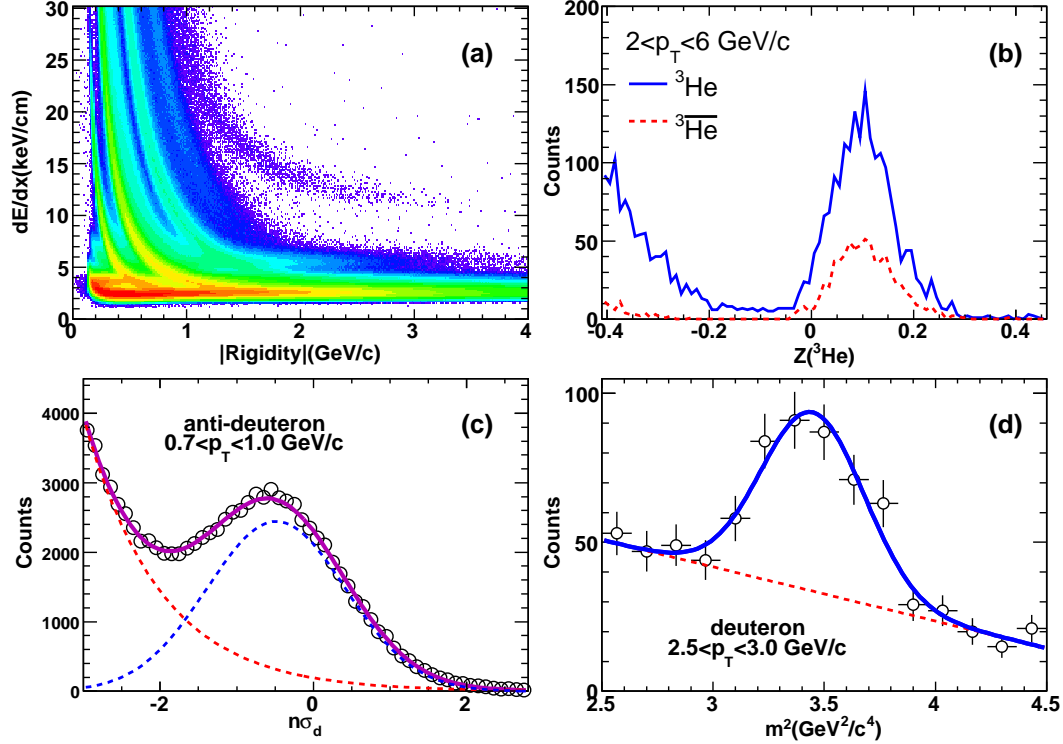


Fig. 1. (a) TPC dE/dx as a function of |rigidity|. (b) Z ($Z = \log((dE/dx)|_{\text{measure}}/(dE/dx)|_{\text{predict}})$) distribution of ${}^3\text{He}$ (solid line) and ${}^3\overline{\text{He}}$ (dashed line). (c) $n\sigma_d$ distribution of \bar{d} at $0.7 < p_T < 1.0$ GeV/c with a Gaussian fit plus an exponential background. (d) The distribution of squared mass ($m^2 = (p/\beta/\gamma)^2$) for d from the TOF after TPC dE/dx selections at $2.5 < p_T < 3.0$ GeV/c, with a Gaussian fit plus a linear background.

model and is described in Ref. [18]. Measurements of the ionization energy loss (dE/dx) of charged tracks in the TPC gas are used to identify protons, deuterons, ${}^3\text{He}$ and their anti-particles. By combining the particle identification capability of dE/dx from the TPC and velocity from the TOF, pions and protons can be identified in $0.3 < p_T < 12$ GeV/c [19,7]. In our analysis, deuterons and anti-deuterons are identified by TPC for $p_T < 1$ GeV/c and by TOF in the range $1 < p_T < 4$ GeV/c. However, at low p_T (< 1 GeV/c), primary deuterons are overwhelmed by background from knock-out deuterons from the beam pipe and inner detector material, which are difficult to separate from collision products. As a result, only anti-deuterons are counted as collision products. Because the absorption effect and detector efficiency for \bar{d} at $p_T < 1$ GeV/c are not well simulated in GEANT, and other produced particles in the same event produce large deuteron background from detector material and beam pipe, only identified \bar{d} in this p_T range are used for elliptic flow calculation. The TPC is used to identify ${}^3\text{He}$ and ${}^3\overline{\text{He}}$ in the range $2 < p_T < 6$ GeV/c.

Figure 1 illustrates the particle identification techniques and methods. Panel

(a) shows the dE/dx of charged tracks as a function of $|\text{rigidity}|$ ($\text{rigidity} = \text{momentum}/\text{charge}$) measured by the TPC at $-1 < \eta < 1$. Panel (b) shows Z ($Z = \log((dE/dx)|_{\text{measure}}/(dE/dx)|_{\text{predict}})$) distribution for ${}^3\text{He}$ and $\overline{{}^3\text{He}}$ signals, where $(dE/dx)|_{\text{predict}}$ is a function accounting for the curvature of dE/dx versus momentum [19,20]. With tight track quality selections imposed by requiring the number of TPC points in a track to be greater than 25 and the distance of closest approach to the event vertex to be less than 1 cm, the ${}^3\text{He}(\overline{{}^3\text{He}})$ signals are essentially background free. Panel (c) shows $n\sigma_d$ (standard Gaussian deviation from $(dE/dx)|_{\text{predict}}$) distribution for \overline{d} at $0.7 < p_T < 1.0$ GeV/c. The signal was fit with a Gaussian function and an exponential background. As can be seen in panels (b) and (c) of Figure 1, the peak centroids in Z and $n\sigma_d$ are shifted from zero. The large shift in ${}^3\text{He}$ is related to the higher ionization density for particles with charge number >1 . See Ref. [21] and Fig. 14 of Ref. [20]. It may be changed by the effects during ion collection. Since this offset does not affect the extracted yields, no attempt was made to more carefully match the overall magnitude of dE/dx . Panel (d) shows m^2 distribution for d at $2.5 < p_T < 3.0$ GeV/c measured by the TOF after the dE/dx cut ($|n\sigma_d| < 2$, in which $n\sigma_d$ denotes the standard Gaussian dE/dx deviation from the expected deuteron value.) [7,19]. The signal was fit with a Gaussian function plus a linear background. The acceptance and tracking efficiencies were studied by Monte Carlo GEANT simulations of the STAR detector [16].

3 Results

3.1 Spectra and the coalescence parameters

The blast-wave (BW) model has been successfully applied to reproduce the π , K , p , and Λ spectra [7], and elliptic flow as well as π HBT correlations as a function of transverse momentum and centrality [6]. This model calculates particle production properties by assuming a parameterized fireball expansion after the collision. The model also assumes local thermal equilibrium with an expansion velocity profile as a function of transverse radius, modulated by an azimuthal density distribution [6]. Predictions from this model for nucleus yields and elliptic flow were compared to our data. Figure 2 shows the p_T spectra of $d(\overline{d})$ and ${}^3\text{He}(\overline{{}^3\text{He}})$. The parameters obtained from using the blast-wave model [6] to describe the spectra and v_2 of π , K , p are used to calculate $d(\overline{d})$ and ${}^3\text{He}(\overline{{}^3\text{He}})$ spectra, with the results shown in Figure 2. The spectra and v_2 of π , K , p are described simultaneously by a single set of parameters, which is shown in Table 1 (only the 0-80% centrality parameters are shown in the table). In the BW model, the nuclei are simply treated as heavier particles emitted from the fireball. The parameters used in the BW description are

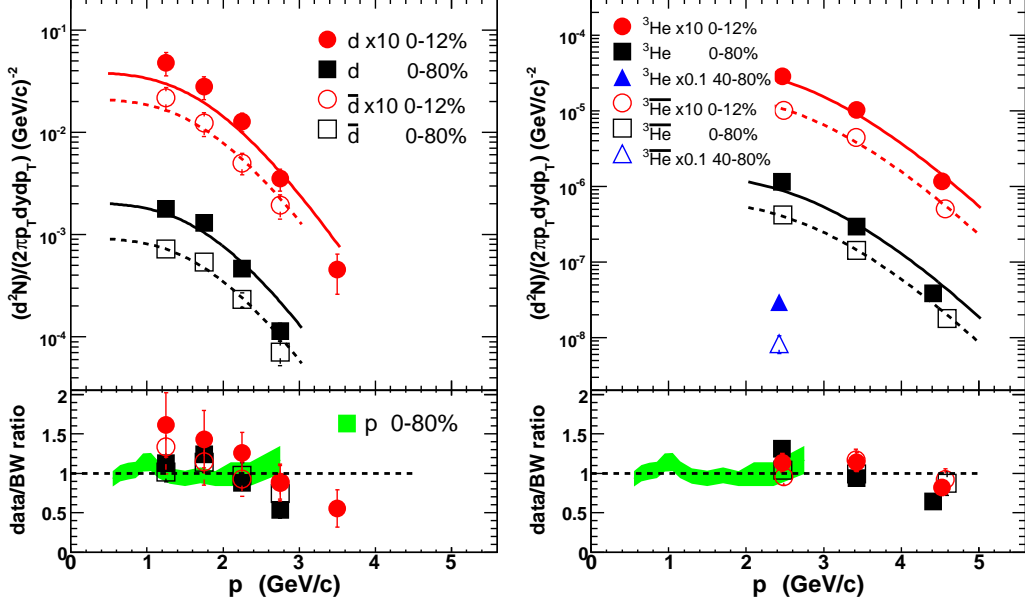


Fig. 2. The left (right) plot shows d and \bar{d} (${}^3\text{He}$ and $\bar{{}^3\text{He}}$) spectra, with a comparison to the blast-wave model calculations. In each plot, the upper panel shows the p_T spectra, with the solid symbols and open symbols representing the particles and anti-particles, respectively. The corresponding blast-wave calculations are shown by solid and dashed lines. The lower panel in each plot shows the data divided by the blast-wave calculation. The bands show the same ratio for protons. Errors are statistical only.

T , ρ_0 , ρ_2 , R_x/R_y , τ_0 and $\Delta\tau$, where T is the temperature. The freeze-out distribution is assumed to be infinite along the beam direction (z direction) and elliptical in the transverse direction (x - y plane), R_x and R_y giving the radii of the ellipse. The parameters ρ_0 and ρ_2 are the zeroth and second order factor of the flow boost along the direction perpendicular to the transverse ellipse, respectively. The source is assumed to emit particles over a finite duration in longitudinal freeze-out proper time ($\tau = \sqrt{t^2 - z^2}$) peaked at τ_0 with a Gaussian distribution width $\Delta\tau$. A more detailed description and definition of the parameters and the BW formulae are given in Ref [6].

In general, the spectra are similar to the model calculations. The ratio between data and model is shown in the bottom panels of Figure 2. The model calculation tends to give harder spectra than seen in the data. This indicates that the coalescence process results in nuclei p_T spectra which do not follow the simple mass dependence expected in the BW model, implying a deviation from simple thermal production.

Table 1

BW parameters: see text for details.

$T(\text{MeV})$	ρ_0	ρ_2	R_x/R_y	$\tau_0(\text{fm}/c)$	$\Delta\tau(\text{fm}/c)$
124.2	0.88	0.061	0.89	9.2	0.03

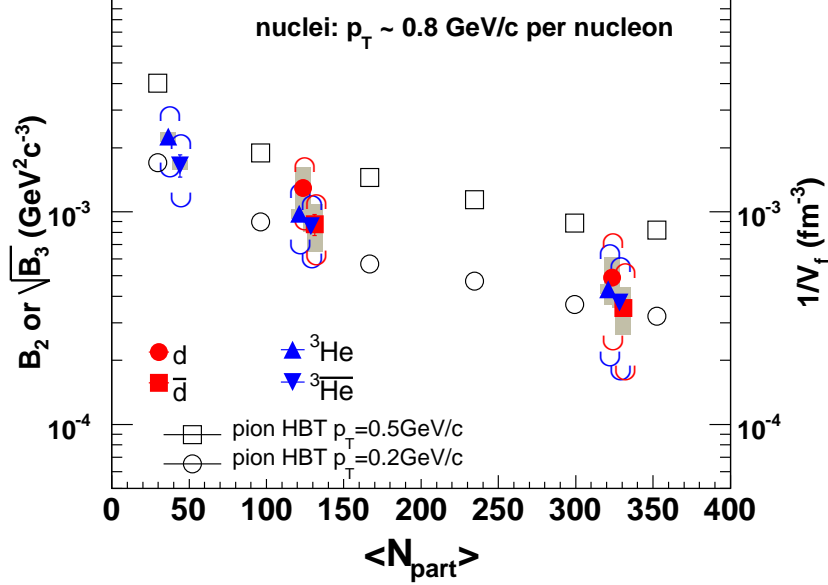


Fig. 3. B_2 and $\sqrt{B_3}$ together with π^\pm HBT volume as a function of collision centrality ($\langle N_{part} \rangle$) in Au+Au collisions. HBT volume is calculated from the HBT correlation lengths along the longitudinal and transverse directions. The gray bands represent systematic errors and the brackets show the uncertainties from the feed-down estimation.

Figure 3 shows the coalescence parameters B_2 and $\sqrt{B_3}$, which are derived from $p(\bar{p})$, $d(\bar{d})$ and ${}^3He(\bar{{}^3He})$ spectra by Equation 1. Here the proton and anti-proton spectra are taken from Ref. [7]. The $p(\bar{p})$ spectra have been corrected for feed-down from $\Lambda(\bar{\Lambda})$ and Σ^\pm weak decays [7]. As mentioned before, $B_A \propto V_f^{1-A}$, so $B_2 \propto 1/V_f$ and $B_3 \propto 1/V_f^2$. Therefore B_2 for $d(\bar{d})$ should be proportional to $\sqrt{B_3}$ for ${}^3He(\bar{{}^3He})$ if the correlation volumes for $d(\bar{d})$ and ${}^3He(\bar{{}^3He})$ are similar. Both B_2 and B_3 show strong centrality dependence. In more central collisions, the smaller coalescence parameter indicates that the correlation volume at thermal freeze-out is larger than for peripheral collisions. This also means that the correlation length in nucleus coalescence grows with the system size.

Figure 3 also shows a comparison with the results of pion HBT data. To calculate the freeze-out volume from HBT measurements, we use the following expression:

$$V_f = (2\pi)^{3/2} \times R_{long} \times R_{side}^2$$

where V_f is the freeze-out volume [2] and R_{long} and R_{side} are the longitudinal and sideward radii, respectively, assuming a density distribution of Gaussian shape in all three dimensions. The R_{long} and R_{side} values are taken from Ref. [6,22] ($k_T = 0.2$ GeV/c). The $d(\bar{d})$ and ${}^3He(\bar{{}^3He})$ transverse momentum ranges are $1.5 < p_T < 2.0$ GeV/c and $2.0 < p_T < 2.5$ GeV/c, respectively. The

HBT data is chosen at the closest p_T to the p_T/A for the nuclei coalescence data throughout all of the centrality bins. The observations that the B_2 and $\sqrt{B_3}$ coalescence parameters are proportional to $1/V_f$ from pion HBT over the full range of centrality considered indicates that the freeze-out volume for the nuclei is closely related to that for pions.

In the coalescence model [2], the proportionality factors quantitatively connecting the B_2 and B_3 parameters to the homogeneous volume depend on flow profile, temperature, correction factors due to quantum wave functions, and other detailed assumptions of the coalescence models. A precise extraction of these model-dependent factors from data will be possible in the future when the large uncertainty on B_2 and B_3 is reduced with the improvement of weak-decay feed-down correction to the proton yields [7].

3.2 Elliptic flow parameter v_2

The elliptic flow parameter, v_2 , is the second order Fourier coefficient of the azimuthal distribution of the produced nuclei relative to the reaction plane of the initial nucleus-nucleus collision. The event-plane method was used to obtain the v_2 of nuclei [23], with the event plane resolution used for correction (calculated using the sub-event method [23]) of 76% for minimum bias triggered events and 68% for central triggered events. In the following discussions only statistical errors will be shown since the low statistics for deuteron and helium nuclei result in these errors being much larger than the estimated systematic errors.

Figure 4 panel (a) shows v_2 as a function of p_T for $d + \bar{d}$, ${}^3He + \overline{{}^3He}$ and \bar{d} in minimum-bias collisions. The results with both v_2 and p_T scaled by A are shown in panel (b). As mentioned in the previous subsection, the π , K , p spectra and v_2 are all described by a single set of blast-wave parameters and then the spectra and v_2 of $d(\bar{d})$, ${}^3He(\overline{{}^3He})$ are calculated. The blast-wave results for the deuteron (3He) v_2 are shown as the solid (dashed) line. As a comparison, the \bar{p} and $\Lambda + \bar{\Lambda}$ v_2 [22] are superimposed on the plot. Results for deuteron v_2 from coalescence and dynamic models [12] are also shown. The data suggest that the $d + \bar{d}$ and baryon v_2 seem to follow the A scaling within errors, indicating that the $d + \bar{d}$ are formed through the coalescence of $p(\bar{p})$ and $n(\bar{n})$ just before thermal freeze-out. However, the scaled ${}^3He + \overline{{}^3He}$ v_2 appears to deviate a bit more from the blast-wave calculated v_2 . To quantify the degree of agreement with the scaling, we performed a χ^2 analysis by comparing the nucleus v_2 to the curves which describe the baryon data. The χ^2 per degree of freedom for deuteron v_2 is 3.1/2 while that of $\overline{{}^3He}$ is 4.1/2. There appears to be a slightly larger deviation for heavier elements.

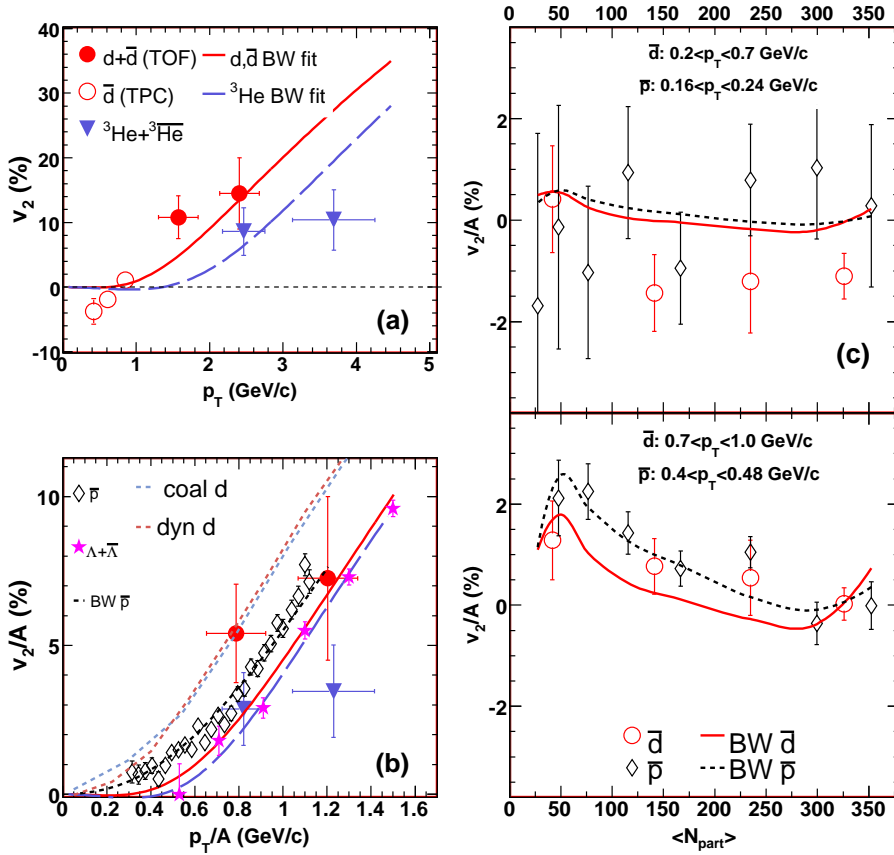


Fig. 4. (a) The elliptic flow parameter v_2 from minimum bias collisions as a function of p_T for ${}^3\text{He} + {}^3\bar{\text{He}}$ (triangles), $d + \bar{d}$ (filled circles), and \bar{d} (open circles); the solid (dashed) line represents the deuteron (${}^3\text{He}$) v_2 calculated by the blast-wave model. (b) $d + \bar{d}$ and ${}^3\text{He} + {}^3\bar{\text{He}}$ v_2 as a function of p_T , both v_2 and p_T have been scaled by A . Errors are statistical only. \bar{p} (open diamonds) and $\Lambda + \bar{\Lambda}$ (solid stars) v_2 are shown in the plot as a comparison. Coalescence and dynamic simulation for deuteron from Ref. [12] are also shown. (c) Low p_T \bar{d} v_2/A (open circles) as a function of centrality fraction (0–10%, 10–20%, 20–40%, 40–80%, respectively). Errors are statistical only. \bar{p} v_2 is also shown as open diamonds. Blast-wave calculations are shown as solid (\bar{d}) and dashed lines (\bar{p}). The 2 subpanels are for different p_T ranges.

The anti-deuteron v_2/A as a function of centrality fraction is shown in Figure 4 panel (c). The upper and lower sub-panels represent results for two different regions of p_T . The \bar{d} is observed to have a negative v_2 in central and mid-central collisions in the transverse momentum range of $0.2 < p_T < 0.7$ GeV/c. This negative v_2 is consistent with a large radial flow, as the blast-wave calculations show. At the same p_T/A where the \bar{d} is negative, the \bar{p} v_2 is consistent both with zero and with the \bar{d} v_2 , due to the large uncertainties. The blast-wave parameters published in Ref. [22] are used to calculate \bar{p} and \bar{d} flow and the calculated results are shown in the figure. The p_T ranges of the \bar{p} data points are selected to match approximately the same p_T/A center of the \bar{d} points used here. Though the blast-wave model predicts the generic feature of negative

v_2 , quantitative agreement between data and model throughout the entire centrality and p_T range is lacking.

3.3 Baryon density at $\mu_B = 0$

As discussed in the introductory section, the d/p ratio is proportional to baryon density. In the collider configuration, the production of low- p_T deuterons is often overwhelmed by background deuterons from the interaction of energetic hadrons (pions and protons) with detector material close to the beam (beam pipe, etc.). When the net baryon density is close to zero, anti-deuterons can be used as a measure of deuteron production. Reference [5] shows that the baryon density in γp , pp , pA and AA collisions follows a universal distribution as a function of beam energy and can be described by statistical processes. At zero baryon chemical potential ($\mu_B = 0$), the d/p ratio and the \bar{d}/\bar{p} ratio are identical and the measurements from all systems considered are consistent with each other. For the 5 data points, which are closest to the $\mu_B = 0$ condition (Au+Au collisions at $\sqrt{s_{NN}} = 200$ GeV (1 point from STAR and the other from PHENIX), $e^+e^- \rightarrow ggg$ at $\sqrt{s} = 10$ GeV, γp at $\sqrt{s} = 200$ GeV, and $\bar{p} + p$ at $\sqrt{s} = 1.8$ TeV), the average value is $\bar{d}/\bar{p} = (7.6 \pm 0.8) \times 10^{-4}$. We note that the D/H value of $(2.8 \pm 0.2) \times 10^{-5}$ obtained from Big Bang nucleosynthesis in the evolution of the Universe [9,10] is about 4% of what is obtained in higher energy processes.

4 Summary

Using the particle identification capabilities of the STAR TPC and TOF detectors, we have measured the $d(\bar{d})$ and ${}^3He(\overline{{}^3He})$ p_T spectra. The extracted coalescence parameters B_2 and $\sqrt{B_3}$ have similar values. They have smaller values for more central collisions, which is consistent with an increasing source size with an increase in collision centrality. The nuclei coalescence parameters are proportional to the inverse of the freeze-out volume estimated using the pion HBT radii in all centrality classes. The spectra of nuclei with $A = 2$ and 3 are in general described by the blast-wave model, which was used to describe the spectrum, elliptic flow, and HBT results. However, the model overpredicts the radial flow, which implies that the coalescence process is different from the simple mass effect as assumed in the blast-wave model.

We have also measured the v_2 of $d(\bar{d})$ and ${}^3He(\overline{{}^3He})$. The v_2 values of $d(\bar{d})$ when scaled by atomic mass number A , follows the baryon v_2 , thereby providing evidence of $d(\bar{d})$ formation through final-state coalescence of nucleons. We also observed the v_2 for \bar{d} to be negative at low p_T in the mid-central collisions.

Comparison with blast-wave calculations shows this is consistent with a large radial flow in Au+Au collisions at a small impact parameter.

5 Acknowledgments

We thank the RHIC Operations Group and RCF at BNL, and the NERSC Center at LBNL and the resources provided by the Open Science Grid consortium for their support. This work was supported in part by the Offices of NP and HEP within the U.S. DOE Office of Science, the U.S. NSF, the Sloan Foundation, the DFG cluster of excellence ‘Origin and Structure of the Universe’, CNRS/IN2P3, RA, RPL, and EMN of France, STFC and EPSRC of the United Kingdom, FAPESP of Brazil, the Russian Ministry of Sci. and Tech., the NNSFC, CAS, MoST, and MoE of China, IRP and GA of the Czech Republic, FOM of the Netherlands, DAE, DST, and CSIR of the Government of India, the Polish State Committee for Scientific Research, and the Korea Sci. & Eng. Foundation.

References

- [1] H.H. Gutbrod *et al.*, Phys. Rev. Lett. **37**, 667 (1976).
- [2] R. Scheibl and U. Heinz, Phys. Rev. C **59**, 1585 (1999); W.J. Llope *et al.*, Phys. Rev. C **52**, 2004 (1995).
- [3] H. Sato and K. Yazaki, Phys. Lett. B **98**, 153 (1981).
- [4] S.T. Butler and C.A. Pearson, Phys. Rev. **129**, 836 (1963).
- [5] H. Liu and Z. Xu, nucl-ex/0610035.
- [6] F. Retiere and M. Lisa, Phys. Rev. C **70**, 044907 (2004).
- [7] B.I. Abelev *et al.* (STAR Collaboration), Phys. Rev. Lett. **97**, 152301 (2006).
- [8] F.Q. Wang and N. Xu, Phys. Rev. C **61**, 021904 (2000); F.Q. Wang, Phys. Lett. B **489**, 273 (2000); P.J. Siemens and J.I. Kapusta, Phys. Rev. Lett. **43**, 1486 (1979); **43**, 1690(E) (1979); L.P. Csernai and J.I. Kapusta, Phys. Rep. **131**, 223 (1986).
- [9] S. Burles, K. M. Nollett, and M.S. Turner, Astrophys. J. **552**, L1 (2001).
- [10] B.D. Fields and S. Sarkar, astro-ph/0601514; W.-M. Yao *et al.* (Particle Data Book), J. Phys. G **33**, 2006 (1).

- [11] S. A. Voloshin, Nucl. Phys. A715, 379 (2003); D. Molnar and S. A. Voloshin, Phys. Rev. Lett. **91**, 092301 (2003); R. C. Hwa and C. B. Yang, Phys. Rev. C **67**, 064902 (2003); R. J. Fries, B. Muller, C. Nonaka, and S. A. Bass, Phys. Rev. Lett. **90**, 202303 (2003).
- [12] Y.S. Oh and C.-M. Ko, Phys. Rev. C **76**, 054910 (2007).
- [13] J.-Y. Ollitrault, Phys. Rev. D **46**, 229 (1992); H. Sorge, Phys. Rev. Lett. **82**, 2048 (1999); K. H. Ackermann *et al.* (STAR Collaboration), Phys. Rev. Lett. **86**, 402 (2001); Tang, A.H., J. Phys. G **31**, S35 (2005).
- [14] C. Adler *et al.* (STAR Collaboration), Phys. Rev. Lett. **87**, 262301 (2001).
- [15] S.S. Adler *et al.* (PHENIX Collaboration), Phys. Rev. Lett. **94**, 122302 (2005); S. Afanasiev *et al.* (PHENIX Collaboration), Phys. Rev. Lett. **99**, 052301 (2007).
- [16] K.H. Ackermann *et al.* (STAR Collaboration), Nucl. Instrum. Methods A **499**, 624 (2003).
- [17] J. Wu *et al.*, Nucl. Instrum. Methods A **538**, 243 (2005); J. Adams *et al.* (STAR Collaboration), Phys. Lett. B **616**, 8 (2005).
- [18] B. I. Abelev *et al.* (STAR Collaboration), Phys. Rev. C **79**, 34909 (2009).
- [19] M. Shao *et al.*, Nucl. Instrum. Methods A **558**, 419 (2006).
- [20] H. Bichsel, Nucl. Instrum. Methods A **562**, 154 (2006).
- [21] Y. Xu *et al.*, arXiv:0807.4303v1.
- [22] J. Adams *et al.* (STAR Collaboration), Phys. Rev. C **72**, 014904 (2005).
- [23] S. Voloshin and Y. Zhang, Z. Phys. C **70**, 665 (1996); S.A. Voloshin, V. Koch and H. G. Ritter, Phys. Rev. C **60**, 024901 (1999).